5408 *Biochemistry* **2010,** *49,* 5408–5417
DOI: 10.1021/bi100058w

BIOCHEMISTRY
including biophysical chemistry & molecular biology
Article

Leptospiral Outer Membrane Lipoprotein LipL32 Binding on Toll-like Receptor 2 of Renal Cells As Determined with an Atomic Force Microscope[†]

Shen-Hsing Hsu,[‡] Yueh-Yu Lo,[‡] Jung-Yu Tung,[‡] Yi-Ching Ko,[§] Yuh-Ju Sun,[‡] Cheng-Chieh Hung,[§] Chih-Wei Yang,[§] Fan-Gang Tseng,[∥] Chien-Chung Fu,[⊥] and Rong-Long Pan*[,‡]

[‡]*Department of Life Science and Institute of Bioinformatics and Structural Biology, College of Life Science, National Tsing Hua University, Hsin Chu 30013, Taiwan, Republic of China,* [§]*Department of Nephrology, Kidney Research Center, Chang Gung Memorial Hospital and Chang Gung University, School of Medicine, Taipei 10507, Taiwan, Republic of China,* [∥]*Department of Engineering and System Science, National Tsing Hua University, Hsin Chu 30013, Taiwan, Republic of China, and* [⊥]*Institute of Nano Engineering and Microsystems, National Tsing Hua University, Hsin Chu 30013, Taiwan, Republic of China*

Received January 14, 2010; Revised Manuscript Received May 28, 2010

ABSTRACT: Leptopirosis is a renal disease caused by pathogenic *Leptospira* that primarily infects the renal proximal tubules, consequently resulting in severe tubular injuries and malfunctions. The protein extracted from the outer membrane of this pathogenic strain contains a major component of a 32 kDa lipoprotein (LipL32), which is absent in the counter membrane of nonpathogenic strains and has been identified as a crucial factor for host cell infection. Previous studies showed that LipL32 induced inflammatory responses and interacted with the extracellular matrix (ECM) of the host cell. However, the exact relationship between LipL32-mediated inflammatory responses and ECM binding is still unknown. In this study, an atomic force microscope with its tip modified by purified LipL32 was used to assess the interaction between LipL32 and cell surface receptors. Furthermore, an antibody neutralization technique was employed to identify Toll-like receptor 2 (TLR2) but not TLR4 as the major target of LipL32 attack. The interaction force between LipL32 and TLR2 was measured as approximately 59.5 ± 8.7 pN, concurring with the theoretical value for a single-pair molecular interaction. Moreover, transformation of a TLR deficient cell line with human TLR2 brought the interaction force from the basal level to approximately 60.4 ± 11.5 pN, confirming unambiguously TLR2 as counter receptor for LipL32. The stimulation of CXCL8/IL-8 expression by full-length LipL32 as compared to that without the N-terminal signal peptide domain suggests a significant role of the signal peptide of the protein in the inflammatory responses. This study provides direct evidence that LipL32 binds to TLR2, but not TLR4, on the cell surface, and a possible mechanism for the virulence of leptospirosis is accordingly proposed.

Leptospirosis is one of the most widespread zoonotic diseases in the world caused by *Leptospira*, bringing forth multiple-organ failure (Weil's syndrome), especially of the kidney (*1*, *2*). The major target of Leptospires in kidney is the renal proximal tubular cells, and the pretreatment of *Leptospira shermani* outer membrane proteins (OMPs)[1] would lead to tubulointerstitial nephritis and acute renal malfunction (*2*−*4*). The leptospiral outer membrane contains the antigenic components, including lipoproteins, lipopolysaccharides (LPS), and peptidoglycans (PGN) (*5*). Several virulent factors have been identified from *Lepstospira*, such as the sphingomyelinases, serine proteases, zinc-dependent proteases, collagenase (*6*), LPS (*7*), a newly identified factor H, laminin- and fibronectin-binding proteins (Lsa24 or Len) (*8*−*10*), Loa22 (*Leptospira* OmpA-like lipoprotein) (*11*), Lig (*Leptospira* immunoglobulin-like) proteins (*12*−*14*), and outer membrane lipoprotein 32 (LipL32) (*15*). During the infection of mammals by *Leptospira interrogans*, a high level of LipL32 was expressed, suggesting implicitly it is the predominant antigen (*16*). A line of evidence demonstrated that LipL32 was a lipoprotein with a molecular mass of 26.7 kDa calculated from its DNA sequence but with an observed electrophoretic mobility at ∼32 kDa upon SDS−PAGE (*16*). LipL32 was also called Hap-1 because of its possible involvement in enhancing hemolysis mediated by sphingomyelinase SphH (*17*). LipL32 is a surface-exposed antigen in which its C-terminus could interact with the ECM components of host cells, such as collagen IV and plasma fibronectin (*18*). The crystal structure of LipL32 indicates that LipL32 is a jellyroll fold structure and the calcium ions are important in structural and thermal stability (*19*−*21*). Meanwhile, LipL32 is a Ca^{2+} binding protein with a novel polyD sequence and seven aspartate residues as a surface patch for Ca^{2+} binding (*20*).

[†]This work was supported by the grants from the National Science Council, Taiwan, Republic of China (NSC 97-2311-B-007-002 and 97-2627-M-007-003) and CGMH-NTHU Joint Research (96N2421E1) to R.-L.P.

*To whom correspondence should be addressed: Department of Life Science, Institute of Bioinformatics and Structural Biology, College of Life Science, National Tsing Hua University, Hsin Chu 30013, Taiwan, Republic of China. Phone and fax: 886-3-5742688. E-mail: rlpan@life.nthu.edu.tw.

[1]Abbreviations: AFM, atomic force microscope; APTES, 3-aminopropyltrimethoxysilane; DMEM, Dulbecco's modified Eagle's medium; ECM, extracellular matrix; FCS, fetal calf serum; IPTG, isopropyl 1-thio-β-galactopyranoside; LB, Luria broth; LPS, lipopolysaccharide(s); LTA, lipoteichoic acid; MAPK, mitogen-activated protein kinase; NF-κB, nuclear transcription factor κB; NTA, nitrilotriacetic acid; OMP, outer membrane protein; PBS, phosphate-buffered saline; PGN, peptidoglycan(s); PRR, pattern recognition receptor; TLR, Toll-like receptor; TIR, Toll/IL-1 receptor.

 Published on Web 05/31/2010

The initial interactions between pathogens and host cells induce an innate immune response at the infection site. Furthermore, Toll-like receptors (TLRs) have been shown to play a central role in the recognition of bacterial components (*22*). TLRs contain leucine-rich repeats (LRRs) in the extracellular portion and a Toll/IL-1 receptor (TIR) domain in the cytoplasmic portion (*22*). To date, 11 TLRs have been identified in mammals and linked to the intracellular signal pathways in the expression of numerous inflammatory cytokines, chemokines, costimulatory proteins, and adhesion molecules. TLRs recognize various microbial components that act as virulent factors (*23*). Many ligands for TLRs have been identified (*24*), among which those for TLR2 include presumably lipoproteins, synthetic lipopeptide, LPS, PGN, and lipoteichoic acid (LTA) (*25*). The synthetic lipopeptide Pam_3Cys and Pam_3CSK_4 molecules were found to interact with TLR2, but not TLR4 (*26*, *27*). Moreover, it was suggested TLR2 forms heterodimers with TLR1 or -6 and interacts with its ligands (*28*). The TLR2−TLR1 heterodimer recognizes the triacylated lipoprotein and lipopeptide as confirmed by cocrystallization of the TLR2−TLR1 complex (*29*−*31*). The crystal structure shows TLR2 contains two lipid binding pockets, while TLR1 but one, enabling the heterodimers to connect with the three lipid chains of the triacylated lipopeptide. TLR6 lacking a similar pocket found in TLR1 forms a heterodimer with TLR2 to bind the diacylated lipopeptide (*30*). Therefore, the lipoprotein and lipopeptide were thus considered as the ligands for TLR2.

Recognition of bacterial components by TLRs of the host cells results in cascades of events that activate nuclear transcription factor κB (NF-κB) and mitogen-activated protein kinases (MAPKs), and the induction of chemokines and cytokines (*24*). Renal tubule epithelial cells express TLR1, -2, -3, -4, and -6 on the cell membrane, indicating that some of these TLRs may contribute to the activation of the innate immune response during tubulointerstitial injury (*23*, *32*). However, little is currently known about the role of LipL32 in TLR signaling of renal tubule epithelial cells with the infection of *Leptospira*.

In this study, we functionalized the AFM tip with purified LipL32 to measure its interaction force between the AFM tip and cell surface receptors and to identify the binding target of this pathogenic protein. A human renal proximal tubular cell (HK2 cell) line was used as model system that expressed the functional TLR2 and TLR4, which have been shown to play essential roles in innate immunity. For the identification of the counter receptor of LipL32, antibody neutralization analysis and TLR deficient human embryonic kidney cells (HEK293 cells) (*33*) were employed to verify the target of the LipL32 attack. Our results demonstrate that LipL32 initiates the signal cascade by interacting with TLR2, but not TLR4.

MATERIALS AND METHODS

Reagents. Fetal calf serum (FCS), Dulbecco's modified Eagle's medium (DMEM), and F-12 nutrient mixture (HAM) were each obtained from Invitrogen Corp. (Carlsbad, CA). The anti-TLR2 IgG clone T2.5 neutralizing antibody and isotype mouse IgG conT2 were provided by Cell Science Inc. (Canton, MA). The anti-His tag antibody was purchased from Santa Cruz Biotechnology (Santa Cruz, CA). All other chemicals were supplied by Sigma (St. Louis, MO).

Expression and Purification of LipL32. The LipL32 cDNA (full-length and N-terminally truncated) was cloned from *L. shermani* according to previous reports (*15*, *20*). The pRSETc-LipL32 DNA was subsequently transformed in the expression host cell *Escherichia coli* BL21(DE3) pLys (Novagen, Madison, WI) which was then grown in Luria broth (LB) medium containing 50 μg/mL ampicillin to an OD_{600} of ~0.6. Isopropyl 1-thio-β-galactopyranoside (IPTG, 1 mM) was afterward added to induce the expression of inserted DNA for an additional 4 h at 37 °C. *E. coli* cells were harvested by centrifugation at 4000*g* for 15 min and then sonicated in tip type sonicator for 30 min in phosphate-buffered saline buffer (PBS buffer). The cell debris was discarded after centrifugation at 14000*g* for 30 min, and the supernatant was applied to a Ni^{2+}-nitrilotriacetic acid (NTA) column (Qiagen, Valencia, CA) for affinity chromatography purification. The nonspecific binding proteins were removed versus 80 mM imidazole, and the highly pure LipL32 was eluted by the 250 mM imidazole fraction. The purified LipL32 was dialyzed against PBS buffer to remove imidazole and consequently stored at 4 °C for further use.

Size Exclusion Chromatography, SDS−PAGE, and Western Blot Analysis. A Superdex 200 pg 16/60 column (GE Healthcare, Chalfont St, U.K.) in PBS buffer was used for size exclusion chromatography gel filtration. The purified LipL32 protein (10−15 μg) was injected into the column and the flow rate set at 1 mL/min at 4 °C. The molecular mass of native LipL32 was determined using standard protein markers: ferritin (440 kDa), β-galactosidase (125 kDa), albumin (67 kDa), ovalbumin (43 kDa), chymotrypsinogen A (25 kDa), and ribonuclease A (15 kDa).

Sodium dodecyl sulfate−polyacrylamide gel electrophoresis (SDS−PAGE) was performed as described previously with minor modifications (*34*, *35*). Purified LipL32 and cytosolic fractions were subjected to 12.5% (w/v) SDS−PAGE and visualized with silver staining or then transferred to polyvinylidene difluoride (PVDF) membranes using a semidry Nova Blot apparatus (Amersham Pharmacia Biotech, now GE Healthcare, Buckinghamshire, U.K.). Western blot analysis was conducted utilizing anti-His tag or anti-TLR2 antibodies according to the protocols recommended by the manufacturer. The blot was stained and visualized with the Western Lightning kit (PerkinElmer Life Sciences Inc., Boston, MA).

Cell Culture and Transient Transfection. Immortalized HK2 cells and human embryonic kidney cells (HEK293 cells) were seeded in a Petri dish with 12 mm round glass coverslips in diameter. HK2 cells were cultured in DMEM/Ham's F12 supplemented with 5% (w/v) FCS, 2 mM glutamine, 20 mM HEPES buffer, 0.4 μg/mL hydrocortisone, 5 μg/mL insulin, 5 μg/mL transferrin, and 5 ng/mL sodium selenite at 37 °C in a humidified atmosphere of 5% (v/v) CO_2 as previously described (*33*). HEK293 cells were grown in DMEM supplemented with 10% (w/v) FCS. The cells were transfected with either pUNO-hTLR2 or pUNO empty plasmid (Invitrogen) alone, or in combination using lipofectamine according to the Lipofectamine 2000 transfection protocol (Life Technologies Inc., Carlsbad, CA). Cells were then fixed for AFM measurements using 1% (w/v) glutaraldehyde in PBS (pH 7.4) for 1 h followed by three washes with PBS. The anti-TLR2 antibody was used to confirm the expression of TLR2 on HK2 and HEK293 cells (see Figure S1 of the Supporting Information; cf. ref *33*).

AFM Tip Functionalization. The AFM cantilever made of silicon nitride, OMCL-TR400PSA (Olympus Co. Ltd., Tokyo, Japan), was cleaned by sonication in a series of solvents: 2-propanol, methanol, and deionized water (5 min each), consecutively. The tips were functionalized according to a previous method with several modifications (*36*). In brief, the probes were

transferred into a 2% (v/v) solution of 3-aminopropyltrimethoxysilane (APTES) (Sigma) in toluene for 2 h. Following the silanization process, the tips were sonicated in methanol and deionized water (5 min each), successively. For functionalization, the AFM tips were incubated in a 15% (v/v) solution of glutaraldehyde (Grade II, Sigma) in PBS for 1 h at room temperature. For anchoring proteins, the tips were rinsed with PBS to remove the glutaraldehyde remainders and subsequently incubated with proteins, including purified LipL32, the anti-TLR2 antibody, the anti-TLR4 antibody, and BSA, successively, for 1 h at room temperature. The functionalized AFM tips were then rinsed three times with PBS to remove the unbound proteins and antibodies. These modified tips were stored in PBS buffer at 4 °C until they were used (*36*).

AFM Observation. The functionalized cantilever tips used in this work had a spring constant (k) in the range of 0.02−0.08 N/m as determined from the amplitude of their thermal vibrations. A commercial atomic force microscope (Nanoscope III, Digital Instruments, Santa Barbara, CA) with a J type scanner was employed throughout this study. The force volume software takes a force curve at each of the 400 points during a two-dimensional scan over a sample surface. Force mapping images were composed of 20 × 20 force measurements over each 5 μm × 5 μm region. The X-Y scan size was 150 μm, and the Z scan distance was 5 μm at a rate of 1 Hz. The force applied to the cell surface was kept below 400 pN, under which no significant harm to cells was observed, using a relative trigger mode in all scans. The distance−force curves and force parameters were obtained according to the methods previously described (*37*). For antibody neutralization analysis, the cells were treated with anti-TLR2 or anti-TLR4 antibodies (diluted 1:1000 in PBS) for 1 h followed by five washes with PBS to remove unbound antibodies. For the binding events, force curves from at least three cells with 10 areas on each surface were independently selected for analysis. All the measurements described above were performed with modified tips and showed repeatedly similar results.

RNA Extraction and Reverse Transcriptase Polymerase Chain Reaction (RT-PCR). Total RNA was extracted according to the previous report with minor modifications (*33*). In brief, the guanidinium thiocyanate/phenol/chloroform method (Cinna/Biotecx Laboratories International Inc., Friendwood, TX) was used. The RNA (1 μg) was reversely transcribed using the avian myeloblastosis virus reverse transcriptase (RT AMV, Boehringer Mannheim), and the primers for human CXCL8/IL-8 were 5′-ATGACTTCCAAGCTGGCCGTGGCT-3′ and 5′-TCTCAGCCCTCTTCAAAAACTTCTC-3′.

AFM Force−Distance Analysis. The force mapping data were transformed into force extension curves for each subsection, and the area under the force extension curve was then calculated. For dynamic force analysis, the rupture speed was controlled within the range from 14 to 1400 nm/s. SPIP (Image Metrology A/S, Hørsholm, Denmark) was used for data analysis, and values of extraction force were thus determined with SigmaPlot version 5.0 (SPSS, Chicago, IL). The maximum distribution force was calculated by a Gaussian fit to the force distribution curve. The dynamic profile for maximum distribution force versus the loading rate was obtained from eq 1

$$F^* = (k_B T/\Delta x) \ln(F\Delta x/k_B T \times k_{off}) \quad (1)$$

where F^* is the most probable rupture force, k_B is the Boltzmann constant, T is the temperature, Δx is the potential width of the energy barrier along the direction of the applied force, k_{off} is the natural dissociation rate at zero force, and F is the loading rate (*38*).

RESULTS

LipL32 Overexpression, Purification, and Characterization. To investigate the interaction between LipL32 and the cell surface receptor, LipL32 cDNA was cloned from *L. shermani* and inserted into the pRSET vector for LipL32 protein expression (as indicated in Materials and Methods). The yield of LipL32 protein was approximately 20 mg from 1 L of medium, demonstrating the feasibility of this expression system. Figure 1A shows protein profiles from cells transformed with vectors pRSET and pRSET-LipL32 (lanes 1 and 2, respectively). The molecular mass of the overexpressed LipL32 protein is in the range of 30−40 kDa (lanes 2 and 3). Further purification via the Ni^{2+} column yielded LipL32 with a high homogeneity as a single band on the SDS−PAGE gel (lane 3). The Western blot analysis using the anti-His tag antibody confirmed the expression, purification, and identification of LipL32 (Figure 1A, right panel). Figure 1B depicts the size exclusion chromatography of purified LipL32 at a molecular mass of 32 kDa. Analytical ultracentrifugation further verified LipL32 as a monomer in a native state (data not shown). The purified LipL32 protein thus obtained was suitable for the following studies.

The virulence of LipL32 was measured as the expression level of CXCL8/IL-8 (Figure 2). Full-length LipL32 and truncated LipL32 without the first 20 amino acids on the N-terminus were used to identify the virulence domain of the protein. LOMPS, the leptospiral outer membrane protein extracts prepared by Triton X-114 solubilization (*2*, *33*), contained primarily LipL32 (data not shown; cf. ref *16*) and consequently could stimulate the expression level of CXCL8/IL8. LOMPS were thus employed as the positive control, while PBS buffer alone was employed as the mock in this study (Figure 2A). The induction of CXCL8/IL-8 by LipL32 follows a dose-dependent route with a level of expression 4.6-fold greater with 500 μg of full-length LipL32 than that of the mock (Figure 2B). However, the response to truncated LipL32 was brought only to 1.3-fold under similar conditions (Figure 2A). The higher level of expression of CXCL8/IL8 by full-length LipL32 versus the truncated form suggests that the N-terminus of LipL32 presumably plays a critical role in inflammatory responses.

Analysis of Force−Distance Curves on the Cell Surface. The AFM force−distance curves for living cells using protein-modified tips implicated the localization and distribution on the cell surface of the receptors being studied (*37*). The traces recorded with an AFM as shown in Figure 3 depict force−distance curves for possible protein−protein interaction at a specific site on the living cell surface. A typical force−distance curve was generated by a noncoated (control) AFM tip approaching and retracting from a particular site on the cell surface without any specific and nonspecific interactions, respectively (Figure 3A,B). Furthermore, observation of the force−distance relationship of the LipL32-coated AFM tip at a specific site on the cell surface yielded two kinds of retraction curves. A similar smooth curve in Figure 3C denotes that the LipL32-coated AFM tip had no interaction with the contacted site on the cell surface like the control tip did. This relatively flat force curve occurs only when there is no interacting receptor on the cell surface for binding protein modified on the AFM tip.

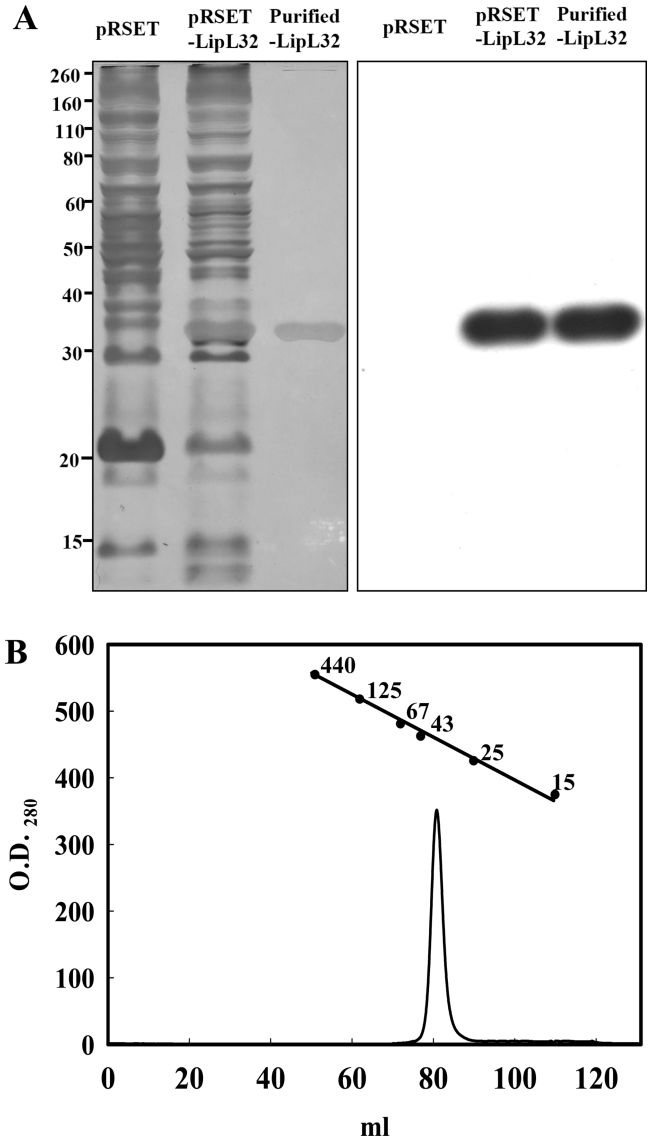

FIGURE 1: Purification and characterization of LipL32. (A) SDS–PAGE and Western blot of cytosolic fractions and purified His-tagged LipL32. The left panel shows SDS–PAGE. The positions of standard molecular mass markers (kilodaltons) are shown at the left: lane 1, cytosolic fraction from cells containing expression vector pRSET; lane 2, cysolic fraction from cells overexpressing LipL32; lane 3, purified His-tagged LipL32. The molecular mass of LipL32 is ~32 kDa. The right panel shows the Western blot of LipL32. The anti-His tag antibody was used to recognize and confirm the purified protein. (C) Size exclusion chromatography of purified LipL32. The molecular mass of purified LipL32 was determined by using a Superdex 200 pg 16/60 column, and the standard markers were ferritin (440 kDa), β-galactosidase (125 kDa), albumin (67 kDa), ovalbumin (43 kDa), chymotrypsinogen A (25 kDa), and ribonuclease A (15 kDa). This result suggests purified LipL32 is monomeric in the native state.

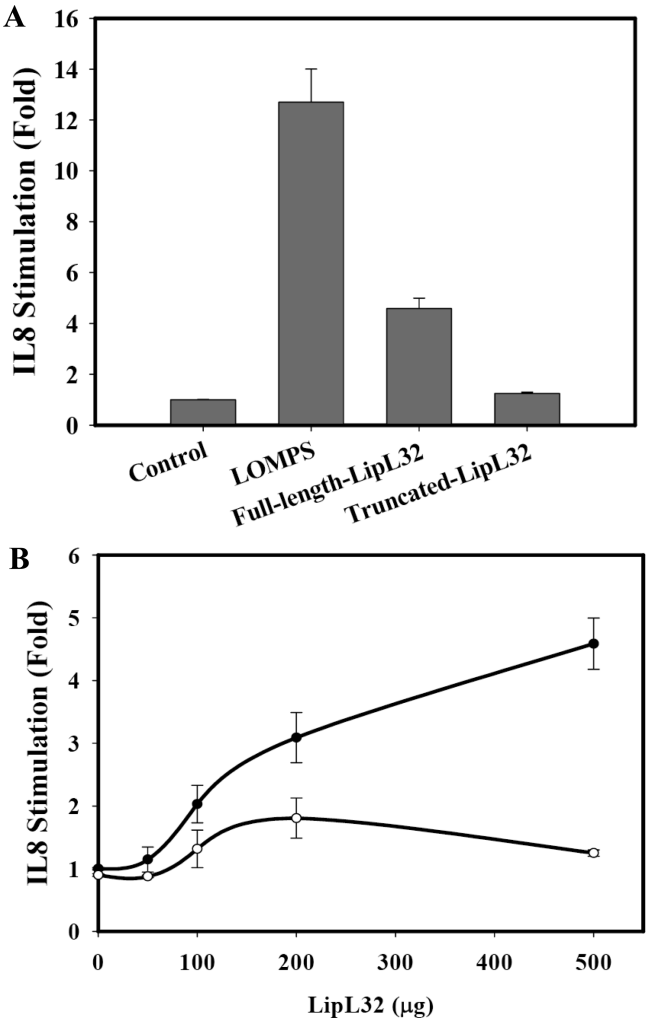

FIGURE 2: Inflammatory responses induced by interaction of LipL32 with TLR2. (A) The stimulation of CXCL8/IL-8 expression by LipL32. LOMPS denote *Leptospira* outer membrane proteins extracted by Triton X-114, while full-length LipL32 and truncated LipL32 were LipL32 with and without the 20 amino acids at the N-terminus, respectively. PBS buffer was used as the mock. (B) Dose dependence of CXCL8/IL-8 stimulation by LipL32. Full-length LipL32 stimulated CXCL8/IL-8 expression by 4.6-fold, while truncated LipL32 stimulated CXCL8/IL-8 expression by 1.3-fold with 500 μg of protein: (●) full-length LipL32 and (○) truncated LipL32.

In contrast, the trough in the force curve in Figure 3D illustrates the extra force exerted for the specific interaction between proteins coated on the AFM tip and the component at the site on the cell surface upon retraction of the tip. More force was used by the AFM tip ~100–200 nm from the cell surface, demonstrating clearly that a specific interaction exists between the coating protein and the cell surface components. An appropriate explanation for this force–distance curve is that the cell surface of HK2 cells contains a receptor component for LipL32 of *L. shermani*. At the moment the AFM tip touched the soft cell surface, the tip protruded approximately 50 nm into the surface (Figure 3; cf. ref *39*). However, when the contact tip was lifted up reciprocally, more force was applied to overcome the interaction between LipL32 on the tip and the receptor at the cell surface (Figure 3D). The extent of the force trough was the interaction force for separating LipL32 from its receptor at the cell surface. In other words, the trough along the force–distance curve presumably reveals the existence of the LipL32 receptor on the cell surface when the tip is accordingly modified. We are thus convinced that this system was feasible for measurement of the interaction force in the following studies. The interaction force in each measurement was determined by the depth at a distance of ~100–200 nm on force–distance curves (Figure 4C). Nevertheless, to ensure the binding event is the specific interaction between the LipL32-modified tip and the TLR2 molecules on the cell surface, the bare AFM tip was treated similarly (Figure 5A). These interaction forces were less than 40 pN and considered for nonspecific interaction (*40*) or for the still known interaction of LipL32 with other ECM molecules (*18*, *20*). Regardless, the cells

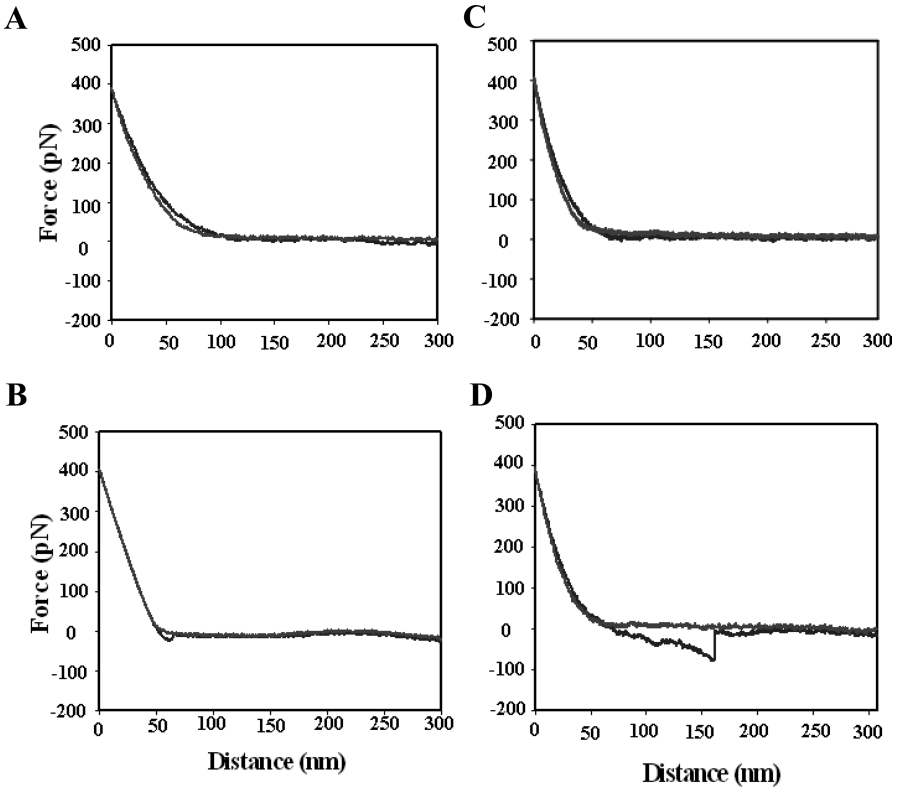

FIGURE 3: Force−distance curves of protein−protein interaction on the living cell surface. (A) Force−distance curves for the bare (control) tip on the cell surface. The gray curve indicates the approach of the AFM tip to the cell surface and the black curve the retraction of the tip from the cell surface. No interaction was observed. (B) Force−distance curves for nonspecific interaction on the cell surface. (C) Force−distance curve showing no interaction between the LipL32-coated AFM tip and the cell surface. (D) Force−distance curve showing the specific interaction between LipL32-modified AFM tips and the cell surface. In all panels, gray indicates approach and black retraction.

were not damaged during the course of these force spectroscopy experiments (cf. Figure S2 of the Supporting Information).

Furthermore, an array mode of force measurement was accordingly used to search the interacting components and their location on the cell surface with full-length or truncated LipL32-modified AFM tips as described in Materials and Methods (Figure 4A). The 5 μm × 5 μm region contained 400 force spots, and each value represented the binding force of the corresponding point on the cell surface of HK2 with truncated LipL32 at the tip as shown in Figure 4B. We also demonstrate that 30% of the force spots performed on the cell surface were positive (Table 1). Moreover, the rupture length distribution of full-length and truncated LipL32-modified tips on the surface of HK2 exhibited peaks at 155.9 ± 24.4 and 157.8 ± 30.1 nm, respectively (Figure 4C). The rupture length of these unbinding events depends presumably on the apparent elasticity of the cell as well as the linker modified at the tip in this system (cf. refs *39* and *41*). However, from theoretical calculations for the lengths of linkers used in this study and the size of LipL32, it is believed the effects of moieties at the tip are negligible (see the Supporting Information, and cf. refs *39* and *41*). Moreover, the apparent elasticity of HK2 cells was determined as a Young modulus of 54.2 ± 13.8 kPa at an applied force of 400 pN (data not shown), a value similar to that on human umbilical vein endothelial cells (HUVEC) (*42*). Under these conditions, it is conceivable that the rupture length came probably from this apparent elasticity of the cell being studied. Nevertheless, other possibilities with respect to this rupture length could not be excluded. Regardless, the exact correlation between cell elasticity and single-molecule forces in AFM measurements requires further investigation.

In addition, histogram plots of force distribution show the interaction forces generated in the range between 0 and 140 pN (Figure 5, left panels). However, the interaction forces between 40 and 80 pN generally represent those for specific interaction of single-molecule pairs (Figure 5, right panel, and cf. ref *38*). The specific interaction (maximum distribution) force of a single full-length LipL32-modified tip with a counter receptor on the cell surface was therefore calculated as approximately 63.9 ± 12.4 pN. Similarly, that for a single truncated LipL32-modified tip was 59.5 ± 8.7 pN. Nevertheless, interaction forces of > 80 pN were also found in the statistical analysis. These forces might come randomly from the multipairs of the protein−protein interactions (*36*) or from some LipL32 proteins interacting with other ECM components (*18*, *20*). Furthermore, the binding events occurring in the range of 40−80 pN for full-length and truncated LipL32-modified tips were calculated as approximately 104 ± 12 and 96 ± 18 counts per unit area of HK2 cell surface, respectively (Table 1 and Figure 5B). Taken together, the data suggest the LipL32 might play a significant role in binding to the cell surface and the N-terminal signal peptide is crucially involved in the inflammatory response (Figure 2).

Identification of Cell Surface Receptors. It is well recognized that an antibody could neutralize the protein−protein interaction of its counter antigen (*33*). The antibody neutralization technique was thus used to identify the interaction components of LipL32 on the cell surface. On the plasma membrane, TLR2 signaling and TLR4 signaling were the major pathways for sensing the bacterial infection (*5*). Therefore, anti-TLR2 and anti-TLR4 antibodies (Ab_{TLR2} and Ab_{TLR4}, respectively) were utilized to neutralize these interactions, if any (Figure 5B).

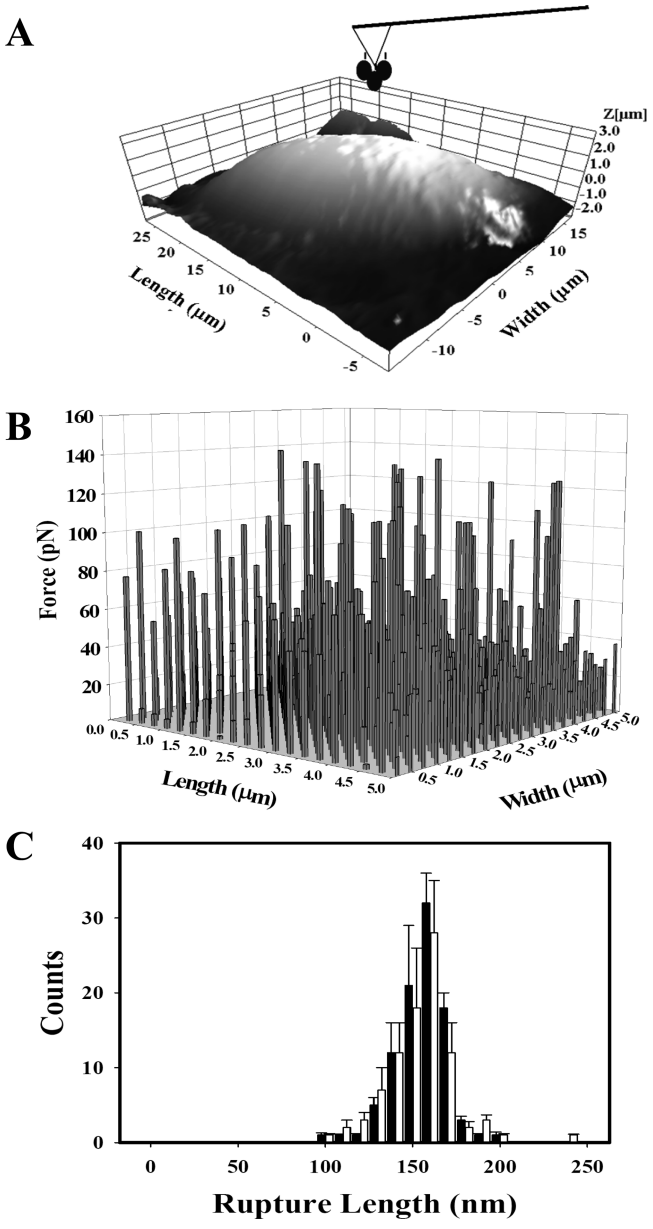

FIGURE 4: Distribution of the interaction force between the LipL32-functionalized AFM tip and the HK2 cell surface. (A) Scheme for measuring the rupture force between the AFM tip and the HK2 cell surface. The AFM tip was modified with purified LipL32 as described in Materials and Methods and applied to the cell surface. (B) Rupture force between the AFM tip and the HK2 cell surface. The LipL32-functionalized AFM tip interacted with the HK2 cell surface in a 5 μm × 5 μm region. The 400 force−distance curves were analyzed, and the force strength was recorded in array mode. (C) Rupture length distribution for LipL32-modified AFM tips on the HK2 cell surface: white for full-length LipL32 and black for truncated LipL32.

Ab_{TLR2} decreased the number of binding events from 96 ± 18 to 16 ± 7 per unit on the HK2 cell surface in the force range (Figure 5B and Table 1). The maximum distribution force could not be calculated appropriately over this force range. In contrast, Ab_{TLR4} decreased the number of binding events to 55 ± 17 per binding unit without a significant change in the maximum distribution force of 58.2 ± 7.6 pN, indicating a neutralization efficiency higher than that of Ab_{TLR4} (Figure 5B and Table 1). The slightly lower extent of Ab_{TLR4} neutralization for binding events might come from the hindrance of the antibody in the vicinity of the receptor being studied. These results here provide direct evidence that LipL32 binds to TLR2, but not TLR4, on the cell surface of the human proximal renal tubule. Nevertheless, the possibility that other components and ECM on the cell surface could interact with LipL32 is not excluded (*18*, *20*).

Furthermore, the TLR2 deficient HEK293 cell line was transformed with vectors pUNO and pUNO-hTLR2 for the confirmation of the interaction between LipL32 and TLR2 (Figure 5C). The existence of TLR2 expression in cells was first verified by a Western blot (Figure S1 of the Supporting Information; cf. ref *33*). Accordingly, force−distance curves using the LipL32-functionalized AFM tip working upon HEK293 cells clearly showed an increase in the number of binding events from 14 ± 5 to 136 ± 20 per unit area as it was transformed by pUNO versus pUNO-hTLR2 (Figure 5C and Table 1). Correspondingly, the force was ~60.4 ± 11.5 pN for the interaction between the LipL32-modified AFM tip and the surface of HEK293 cells transformed with pUNO-hTLR2 (Figure 5C and Table 1). The higher frequency of interaction between the modified tip and the cell surface of overexpressed mutants further validated the interaction of LipL32 with HK2 and HEK293 cell surfaces via TLR2.

In contrast, the antibodies modified on AFM tips were used to confirm the presence of TLR2 and TLR4 on the HK2 cell surface. The specific interaction force was thus obtained (~121.7 ± 13.8 pN) using Ab_{TLR2}-modified AFM tips on the HK2 cell surface (Figure S1 of the Supporting Information and Table 1). The binding force of the antigen−antibody interaction measured with the AFM was ~30−150 pN depending on the different loading rate (*38*, *43*). In this study, the interaction force between TLR and TLR antibodies was ~120 pN, as the positive control (Table 1). The specific interaction force between TLR2 antibody-modified AFM tips and the cell surface was ~121.7 ± 13.8 pN compared to 59.5 ± 8.7 pN for the LipL32-modified AFM tip binding to the cell surface. The TLR2−TLR2 antibody interaction force was ~2-fold stronger than the LipL32−TLR2 interaction force (Table 1). Similarly, the Ab_{TLR2}-modified AFM tip that interacted with the HK2 cell surface decreased the number of binding events from 114 ± 24 to 45 ± 8 per area in the presence of LipL32 (Table 1). The similar neutralization effects of Ab_{TLR2} further demonstrate the interaction between LipL32 and TLR2 on the cell surface.

Dynamic Force Spectroscopy. The rupture force at different loading rates (from 14 to 1400 nm/s) was measured using LipL32-modified AFM tips on the HK2 cell surface (Figure 6). At each loading rate, 400 force curves were collected and analyzed for binding kinetics. The rupture forces fall in the range from 43.6 ± 7.9 to 75.1 ± 15.7 pN at rates from 14 to 1400 nm/s, respectively. However, the rupture forces at the rates below this range could not be measured because of the high background noise, while those at rates higher than 1400 nm/s were beyond the scope of this instrument (data not shown). The maximum distribution force was then determined by a Gaussian fit of the LipL32−TLR2 interaction force at different loading rates in this range. The maximum distribution force was subsequently plotted versus the logarithm of the loading rate, yielding a linear fit of the slope ($k_BT/\Delta x$) that corresponds to an energy barrier of approximately 17.5 pN/nm at Δx = 0.23 nm. Consequently, the dissociation rate at zero force (k_{off}) of approximately 0.24 s^{-1} and the potential width Δx of 0.23 nm were obtained from eq 1 and Figure 6, respectively. The linearity of the dynamic force plot suggests only one energy barrier (i.e., one binding site) for LipL32−TLR2 interaction.

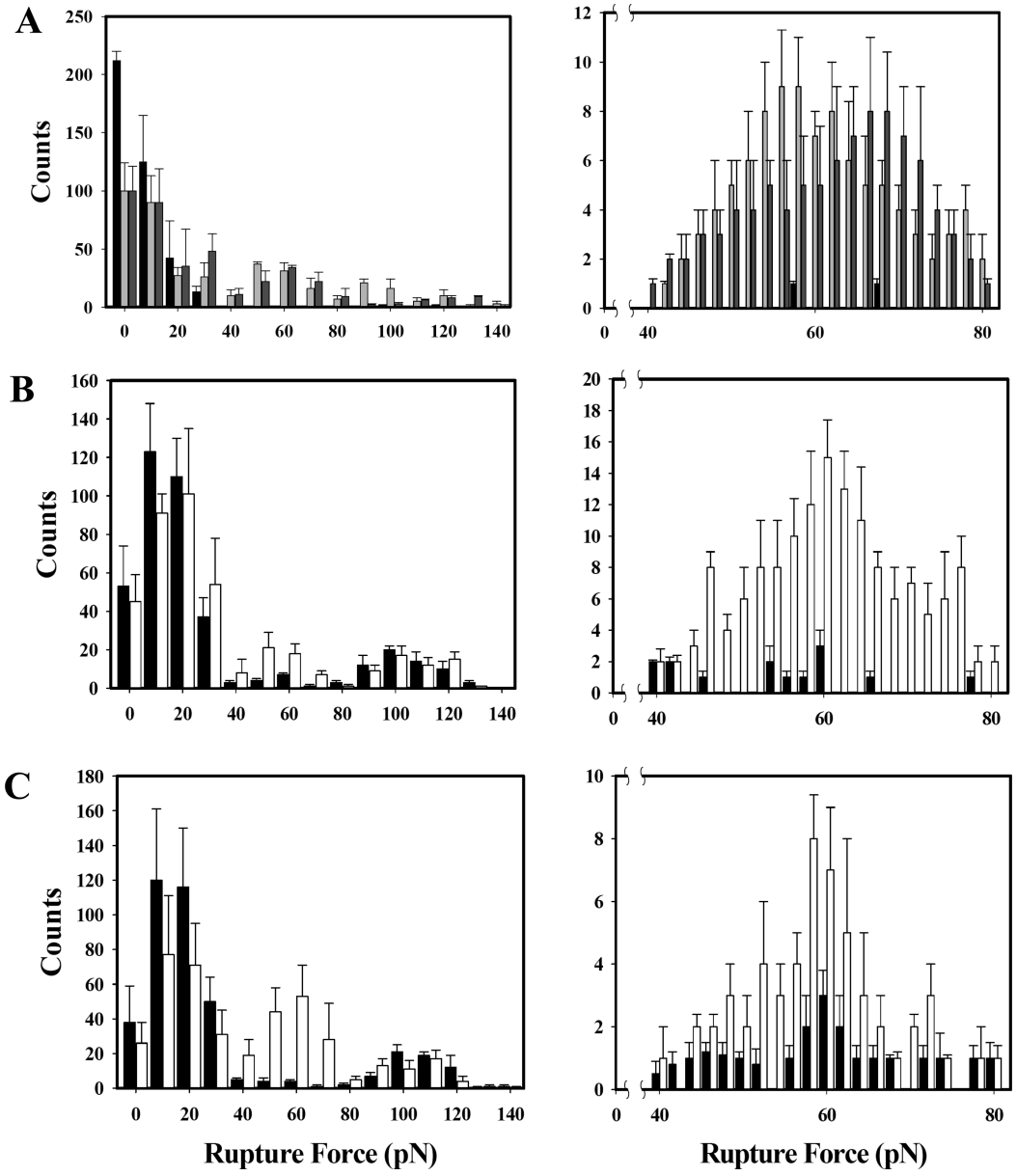

FIGURE 5: Histograms of rupture forces. (A) Rupture forces for tip−cell interactions: black for the bare tip, dark gray for the tip modified with full-length LipL32, and gray for the tip modified with truncated LipL32. The rupture force between 40 and 80 pN displayed a distinct peak with maximum distribution forces of 63.9 ± 12.4 and 59.5 ± 8.7 pN for tips modified with full-length and truncated LipL32, respectively. No obvious maximum distribution force or peak was observed for the bare tip. (B) Rupture forces after antibody neutralization. The Gaussian fit yields a significant peak and a maximum distribution force of 58.2 ± 7.6 pN after Ab_{TLR4} neutralization. No obvious peak or maximum distribution force was obtained after Ab_{TLR2} neutralization: black for Ab_{TLR2} and white for Ab_{TLR4}. (C) Rupture forces for HEK293 cells overexpressing hTLR2: black for pUNO and white for pUNO-TLR2. The Gaussian fit yields a significant peak and a maximum distribution force of 62.1 ± 3.6 pN for HEK293 cells expressing hTLR2, while those for cells with pUNO did not show a significant peak or maximum distribution force: black for pUNO and white for pUNO-TLR2.

DISCUSSION

It has been long believed that leptospirosis is caused by the interaction of OMPs from *Leptospira* with the surface of the host cell (*5*). The most suspicious OMP involved in leptospirosis is LipL32, since it is the most abundant outer membrane protein in pathogenic species of *Leptospira* compared with nonpathogenic ones (*16*, *44*, *45*). However, a recent report on the pathogenesis of LipL32 deficient *Leptospira* denied the involvement of this OMP (*46*). This work demonstrates that LipL32 could directly interact with TLR2 on the host cell surface through which consequent signal cascades might be triggered (*33*).

LipL32 Interacts with TLR2. TLRs contain LRRs responsible for ligand binding (*24*). Furthermore, TLRs could recognize microbial patterns and are thus termed pattern recognition receptors (PRRs) (*22*). Analysis of the crystal structure of the human TLR2−TLR1 lipopeptide complex suggests that LRR domains presumably could interact with lipid molecules of lipoproteins (*30*). In this study, the AFM was used to further verify the possibility of the interaction between LipL32 and TLR2. The AFM is a powerful tool for exploring the forces and dynamics of the interaction between individual ligands and receptors, either as isolated molecules or on cell surfaces. The resolution at the subnanonewton scale provides direct evidence of the existence of a function-related protein residing on the surface of live cells (*42*, *43*, *47*, *48*). This report, for the first time, demonstrates directly the presence of the interaction between

Table 1: Interaction Forces and Binding Events between the AFM Tip and Cell Surface[a]

	interaction force[b] (pN) (no. of binding events[c])				
	tip only	tip with f-LipL32[d]	tip with t-LipL32[d]	tip with Ab_{TLR2}	tip with Ab_{TLR4}
HK2	− (2 ± 1)	63.9 ± 12.4 (104 ± 12)	59.5 ± 8.7 (96 ± 18)	121.7 ± 13.8 (114 ± 24)	105.4 ± 15.3 (121 ± 28)
HK2 with LipL32	− (1 ± 1)	ND	ND	115.4 ± 22.8 (45 ± 8)	129.7 ± 31.6 (108 ± 18)
HK2 with Ab_{TLR2}	− (3 ± 2)	− (14 ± 3)	− (16 ± 7)	ND	112.5 ± 7.1 (75 ± 15)
HK2 with Ab_{TLR4}	− (5 ± 3)	62.5 ± 14.1 (87 ± 11)	58.2 ± 7.6 (55 ± 17)	109.5 ± 11.4 (91 ± 24)	ND
HEK293 without TLR2	− (1 ± 1)	57.4 ± 11.9 (94 ± 10)	60.4 ± 11.5 (136 ± 20)	125.7 ± 15.6 (143 ± 23)	− (12 ± 5)
HEK293 without pUNO	− (2 ± 1)	− (11 ± 4)	− (14 ± 5)	− (7 ± 3)	− (7 ± 2)

[a]The AFM tips were modified with purified LipL32 (full-length and truncated), the anti-TLR2 antibody, and the anti-TLR4 antibody. The HK2 cell surface was treated with various blocking components such as purified LipL32, the anti-TLR2 antibody, and the anti-TLR4 antibody. The force−distance curves were recorded under the conditions described in Materials and Methods. The TLR2 deficient HEK293 cell line transfected with expression vectors pUNO and pUNO-TLR2 was used to measure the interaction forces under the conditions mentioned above. [b]Legend: −, negligible; ND, not determined. [c]The binding events for LipL32-modified AFM tips were captured in the range of 40−80 pN, while those for antibody-modified AFM tips were captured in the range of 100−140 pN. [d]Legend: f, full-length; t, truncated.

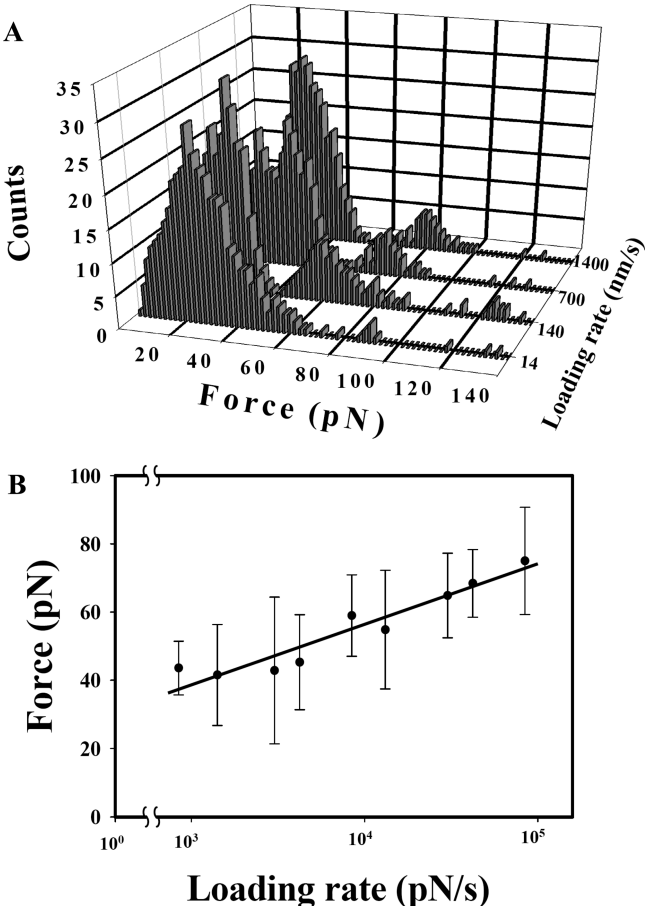

FIGURE 6: Dependence of rupture force on loading rate. (A) Rupture force distribution for the LipL32−TLR2 interaction at different loading rates: lane 1, 14 nm/s; lane 2, 140 nm/s; lane 3, 700 nm/s; lane 4, 1400 nm/s. (B) Dynamic force plot for the LipL32−TLR2 interaction. The maximum distribution force between LipL32 and TLR2 was determined by a Gaussian fit at different loading rates (from 14 to 1400 nm/s). The dynamic force plot is linear, indicating only one energy barrier for LipL32−TLR2 interaction. The line fit according to eq 1 yields a dissociation rate at zero force (k_{off}) of approximately 0.24 s^{-1} and a potential width Δx of 0.23 nm.

LipL32 and TLR2 on the cell surface (Figure 5). The interaction forces of the antibody-modified AFM tip were stronger than those of the LipL32-modified one showing stronger interaction between TLRs and Ab_{TLR}. Moreover, Ab_{TLR2} had a higher neutralization efficiency than Ab_{TLR4}, confirming explicitly that TLR2 is the counter receptor for LipL32 (Figure 5).

The interaction of LipL32 with the cell surface was further verified using TLR2 deficient HEK293 cells. The interaction forces between LipL32 and TLR2 overexpressed on HEK293 cells were similar to those with the HK2 cell surface. However, the binding events were 1.4 times stronger than those with the HK2 cell surface (Figure 5). The Ab_{TLR2}-modified AFM tips and a Western blot against Ab_{TLR2} were used as the positive control to confirm the TLR2 expression on HK2 and HEK293 cells, respectively (Table 1 and Figure S1 of the Supporting Information). These data provide strong evidence that LipL32 interacted with TLR2, but not TLR4.

LipL32 Binding to TLR2. It has been shown that TLR2 recognized bacterial lipoproteins; however, TLR4 recognized LPS of Gram-negative bacteria (*24*). It was demonstrated that TLR2 forms a dimeric structure with TLR1 to interact with the triacylated lipoprotein as the innate immunity against the bacterial infection (*49*). Further analysis of the crystal structure of the TLR2−TLR1 complex with the lipopeptide Pam_3CSK_4 suggests that TLR2 interacted with two lipid molecules and TLR1 with the third one (*30*). This line of evidence indicates the lipoproteins interact with TLR2 at their lipid domain. In this study, it is further shown the LipL32 truncated with the lipobox could still interact with TLR2, providing new insight into the binding sites of LipL32. In addition, we also demonstrated that an ECM molecule, vitronectin, and its receptor, integrin $\beta 3$, contributed to the interaction of the lipoprotein with TLR2 (*50*). However, no direct interaction of LipL32 with vitronectin was found (data not shown). Also, the presence of vitronectin did not assist in the interaction of LipL32 with TLR2 (data not shown). These pieces of evidence further confirm our speculation that LipL32 could directly interact with TLR2. Nevertheless, the domains of LipL32 for interacting with TLR2 require future investigation.

ACKNOWLEDGMENT

We thank professor Lih-Yuan Lin for assistance in cell culture and professor Ming-Jeng Pan for providing the LipL32 clone.

SUPPORTING INFORMATION AVAILABLE

Figures S1 and S2 and theoretical calculations. This material is available free of charge via the Internet at http://pubs.acs.org.

REFERENCES

1. Levett, P. N. (2001) *Leptospirosis. Clin. Microbiol. Rev. 14*, 296–326.
2. Tian, Y. C., Chen, Y. C., Hung, C. C., Chang, C. T., Wu, M. S., Phillips, A. O., and Yang, C. W. (2006) Leptospiral outer membrane

protein induces extracellular matrix accumulation through a TGF-β1/Smad-dependent pathway. *J. Am. Soc. Nephrol. 17*, 2792–2798.
3. Farr, R. W. (1995) *Leptospirosis. Clin. Infect. Dis. 21*, 1–6.
4. Morrison, W. I., Wright, N. G., and Cornwell, H. J. (1976) An immunopathologic study of *interstitial nephritis* associated with experimental canine adenovirus infection. *J. Pathol. 120*, 221–228.
5. Yang, C. W. (2007) *Leptospirosis* renal disease: Understanding the initiation by Toll-like receptors. *Kidney Int. 72*, 918–925.
6. Bulach, D. M., Zuerner, R. L., Wilson, P., Seemann, T., McGrath, A., Cullen, P. A., Davis, J., Johnson, M., Kuczek, E., Alt, D. P., Peterson-Burch, B., Coppel, R. L., Rood, J. I., Davies, J. K., and Adler, B. (2006) Genome reduction in *Leptospira borgpetersenii* reflects limited transmission potential. *Proc. Natl. Acad. Sci. U.S.A. 103*, 14560–14565.
7. Werts, C., Tapping, R. I., Mathison, J. C., Chuang, T. H., Kravchenko, V., Saint Girons, I., Haake, D. A., Godowski, P. J., Hayashi, F., Ozinsky, A., Underhill, D. M., Kirschning, C. J., Wagner, H., Aderem, A., Tobias, P. S., and Ulevitch, R. J. (2001) Leptospiral lipopolysaccharide activates cells through a TLR2-dependent mechanism. *Nat. Immunol. 2*, 346–352.
8. Barbosa, A. S., Abreu, P. A., Neves, F. O., Atzingen, M. V., Watanabe, M. M., Vieira, M. L., Morais, Z. M., Vasconcellos, S. A., and Nascimento, A. L. (2006) A newly identified leptospiral adhesin mediates attachment to laminin. *Infect. Immun. 74*, 6356–6364.
9. Stevenson, B., Choy, H. A., Pinne, M., Rotondi, M. L., Miller, M. C., Demoll, E., Kraiczy, P., Cooley, A. E., Creamer, T. P., Suchard, M. A., Brissette, C. A., Verma, A., and Haake, D. A. (2007) *Leptospira interrogans* endostatin-like outer membrane proteins bind host fibronectin, laminin and regulators of complement. *PLoS One 2*, e1188.
10. Verma, A., Hellwage, J., Artiushin, S., Zipfel, P. F., Kraiczy, P., Timoney, J. F., and Stevenson, B. (2006) LfhA, a novel factor H-binding protein of *Leptospira interrogans*. *Infect. Immun. 74*, 2659–2666.
11. Ristow, P., Bourhy, P., da Cruz McBride, F. W., Figueira, C. P., Huerre, M., Ave, P., Girons, I. S., Ko, A. I., and Picardeau, M. (2007) The OmpA-like protein Loa22 is essential for leptospiral virulence. *PLoS Pathog. 3*, e97.
12. Matsunaga, J., Barocchi, M. A., Croda, J., Young, T. A., Sanchez, Y., Siqueira, I., Bolin, C. A., Reis, M. G., Riley, L. W., Haake, D. A., and Ko, A. I. (2003) Pathogenic *Leptospira* species express surface-exposed proteins belonging to the bacterial immunoglobulin superfamily. *Mol. Microbiol. 49*, 929–945.
13. Palaniappan, R. U., Chang, Y. F., Hassan, F., McDonough, S. P., Pough, M., Barr, S. C., Simpson, K. W., Mohammed, H. O., Shin, S., McDonough, P., Zuerner, R. L., Qu, J., and Roe, B. (2004) Expression of leptospiral immunoglobulin-like protein by *Leptospira interrogans* and evaluation of its diagnostic potential in a kinetic ELISA. *J. Med. Microbiol. 53*, 975–984.
14. Palaniappan, R. U., Chang, Y. F., Jusuf, S. S., Artiushin, S., Timoney, J. F., McDonough, S. P., Barr, S. C., Divers, T. J., Simpson, K. W., McDonough, P. L., and Mohammed, H. O. (2002) Cloning and molecular characterization of an immunogenic LigA protein of *Leptospira interrogans*. *Infect. Immun. 70*, 5924–5930.
15. Yang, C. W., Wu, M. S., Pan, M. J., Hsieh, W. J., Vandewalle, A., and Huang, C. C. (2002) The *Leptospira* outer membrane protein LipL32 induces tubulointerstitial nephritis-mediated gene expression in mouse proximal tubule cells. *J. Am. Soc. Nephrol. 13*, 2037–2045.
16. Haake, D. A., Chao, G., Zuerner, R. L., Barnett, J. K., Barnett, D., Mazel, M., Matsunaga, J., Levett, P. N., and Bolin, C. A. (2000) The leptospiral major outer membrane protein LipL32 is a lipoprotein expressed during mammalian infection. *Infect. Immun. 68*, 2276–2285.
17. Lee, S. H., Kim, K. A., Park, Y. G., Seong, I. W., Kim, M. J., and Lee, Y. J. (2000) Identification and partial characterization of a novel hemolysin from *Leptospira interrogans* serovar lai. *Gene 254*, 19–28.
18. Hauk, P., Macedo, F., Romero, E. C., Vasconcellos, S. A., de Morais, Z. M., Barbosa, A. S., and Ho, P. L. (2008) In LipL32, the major leptospiral lipoprotein, the C terminus is the primary immunogenic domain and mediates interaction with collagen IV and plasma fibronectin. *Infect. Immun. 76*, 2642–2650.
19. Hauk, P., Guzzo, C. R., Roman Ramos, H., Ho, P. L., and Farah, C. S. (2009) Structure and calcium-binding activity of LipL32, the major surface antigen of pathogenic *Leptospira* sp.. *J. Mol. Biol. 390*, 722–736.
20. Tung, J. Y., Yang, C. W., Chou, S. W., Lin, C. C., and Sun, Y. J. (2009) Calcium binds to LipL32, a lipoprotein from pathogenic *Leptospira*, and modulates fibronectin binding. *J. Biol. Chem. 285*, 3245–3252.
21. Vivian, J. P., Beddoe, T., McAlister, A. D., Wilce, M. C., Zaker-Tabrizi, L., Troy, S., Byres, E., Hoke, D. E., Cullen, P. A., Lo, M., Murray, G. L., Adler, B., and Rossjohn, J. (2009) Crystal structure of LipL32, the most abundant surface protein of pathogenic *Leptospira* spp.. *J. Mol. Biol. 387*, 1229–1238.
22. Takeda, K., Kaisho, T., and Akira, S. (2003) Toll-like receptors. *Annu. Rev. Immunol. 21*, 335–376.
23. Anders, H. J., Banas, B., and Schlondorff, D. (2004) Signaling danger: Toll-like receptors and their potential roles in kidney disease. *J. Am. Soc. Nephrol. 15*, 854–867.
24. Akira, S., Takeda, K., and Kaisho, T. (2001) Toll-like receptors: Critical proteins linking innate and acquired immunity. *Nat. Immunol. 2*, 675–680.
25. Schwandner, R., Dziarski, R., Wesche, H., Rothe, M., and Kirschning, C. J. (1999) Peptidoglycan- and lipoteichoic acid-induced cell activation is mediated by Toll-like receptor 2. *J. Biol. Chem. 274*, 17406–17409.
26. Hirschfeld, M., Kirschning, C. J., Schwandner, R., Wesche, H., Weis, J. H., Wooten, R. M., and Weis, J. J. (1999) Cutting edge: Inflammatory signaling by *Borrelia burgdorferi* lipoproteins is mediated by Toll-like receptor 2. *J. Immunol. 163*, 2382–2386.
27. Lien, E., Sellati, T. J., Yoshimura, A., Flo, T. H., Rawadi, G., Finberg, R. W., Carroll, J. D., Espevik, T., Ingalls, R. R., Radolf, J. D., and Golenbock, D. T. (1999) Toll-like receptor 2 functions as a pattern recognition receptor for diverse bacterial products. *J. Biol. Chem. 274*, 33419–33425.
28. Ozinsky, A., Underhill, D. M., Fontenot, J. D., Hajjar, A. M., Smith, K. D., Wilson, C. B., Schroeder, L., and Aderem, A. (2000) The repertoire for pattern recognition of pathogens by the innate immune system is defined by cooperation between Toll-like receptors. *Proc. Natl. Acad. Sci. U.S.A. 97*, 13766–13771.
29. Alexopoulou, L., Thomas, V., Schnare, M., Lobet, Y., Anguita, J., Schoen, R. T., Medzhitov, R., Fikrig, E., and Flavell, R. A. (2002) Hyporesponsiveness to vaccination with *Borrelia burgdorferi* OspA in humans and in TLR1- and TLR2-deficient mice. *Nat. Med. 8*, 878–884.
30. Jin, M. S., Kim, S. E., Heo, J. Y., Lee, M. E., Kim, H. M., Paik, S. G., Lee, H., and Lee, J. O. (2007) Crystal structure of the TLR1-TLR2 heterodimer induced by binding of a tri-acylated lipopeptide. *Cell 130*, 1071–1082.
31. Takeuchi, O., Sato, S., Horiuchi, T., Hoshino, K., Takeda, K., Dong, Z., Modlin, R. L., and Akira, S. (2002) Cutting edge: Role of Toll-like receptor 1 in mediating immune response to microbial lipoproteins. *J. Immunol. 169*, 10–14.
32. Tsuboi, N., Yoshikai, Y., Matsuo, S., Kikuchi, T., Iwami, K., Nagai, Y., Takeuchi, O., Akira, S., and Matsuguchi, T. (2002) Roles of Toll-like receptors in C-C chemokine production by renal tubular epithelial cells. *J. Immunol. 169*, 2026–2033.
33. Hung, C. C., Chang, C. T., Tian, Y. C., Wu, M. S., Yu, C. C., Pan, M. J., Vandewalle, A., and Yang, C. W. (2006) Leptospiral membrane proteins stimulate pro-inflammatory chemokines secretion by renal tubule epithelial cells through Toll-like receptor 2 and p38 mitogen activated protein kinase. *Nephrol., Dial., Transplant. 21*, 898–910.
34. Laemmli, U. K. (1970) Cleavage of structural proteins during the assembly of the head of bacteriophage T4. *Nature 227*, 680–685.
35. Hsu, S. H., Hsiao, Y. Y., Liu, P. F., Lin, S. M., Luo, Y. Y., and Pan, R. L. (2009) Purification, characterization, and spectral analyses of histidine-tagged vacuolar H^+-pyrophosphatase expressed in yeast. *Bot. Stud. 50*, 291–301.
36. Allen, S., Chen, X., Davies, J., Davies, M. C., Dawkes, A. C., Edwards, J. C., Roberts, C. J., Sefton, J., Tendler, S. J., and Williams, P. M. (1997) Detection of antigen-antibody binding events with the atomic force microscope. *Biochemistry 36*, 7457–7463.
37. Kim, H., Arakawa, H., Hatae, N., Sugimoto, Y., Matsumoto, O., Osada, T., Ichikawa, A., and Ikai, A. (2006) Quantification of the number of EP3 receptors on a living CHO cell surface by the AFM. *Ultramicroscopy 106*, 652–662.
38. Neuert, G., Albrecht, C., Pamir, E., and Gaub, H. E. (2006) Dynamic force spectroscopy of the digoxigenin-antibody complex. *FEBS Lett. 580*, 505–509.
39. Madl, J., Rhode, S., Stangl, H., Stockinger, H., Hinterdorfer, P., Schutz, G. J., and Kada, G. (2006) A combined optical and atomic force microscope for live cell investigations. *Ultramicroscopy 106*, 645–651.
40. Ron, A., Singh, R. R., Fishelson, N., Socher, R., Benayahu, D., and Shacham-Diamand, Y. (2008) Site localization of membrane-bound proteins on whole cell level using atomic force microscopy. *Biophys. Chem. 132*, 127–138.
41. Yersin, A., Osada, T., and Ikai, A. (2008) Exploring transferrin-receptor interactions at the single-molecule level. *Biophys. J. 94*, 230–240.

42. Riethmuller, C., Schaffer, T. E., Kienberger, F., Stracke, W., and Oberleithner, H. (2007) Vacuolar structures can be identified by AFM elasticity mapping. *Ultramicroscopy 107*, 895–901.
43. Kienberger, F., Kada, G., Mueller, H., and Hinterdorfer, P. (2005) Single molecule studies of antibody-antigen interaction strength versus intra-molecular antigen stability. *J. Mol. Biol. 347*, 597–606.
44. Picardeau, M., Bulach, D. M., Bouchier, C., Zuerner, R. L., Zidane, N., Wilson, P. J., Creno, S., Kuczek, E. S., Bommezzadri, S., Davis, J. C., McGrath, A., Johnson, M. J., Boursaux-Eude, C., Seemann, T., Rouy, Z., Coppel, R. L., Rood, J. I., Lajus, A., Davies, J. K., Medigue, C., and Adler, B. (2008) Genome sequence of the saprophyte *Leptospira biflexa* provides insights into the evolution of *Leptospira* and the pathogenesis of *leptospirosis*. *PLoS One 3*, e1607.
45. Zuerner, R. L., Knudtson, W., Bolin, C. A., and Trueba, G. (1991) Characterization of outer membrane and secreted proteins of *Leptospira interrogans* serovar *pomona*. *Microb. Pathog. 10*, 311–322.
46. Murray, G. L., Srikram, A., Hoke, D. E., Wunder, E. A., Jr., Henry, R., Lo, M., Zhang, K., Sermswan, R. W., Ko, A. I., and Adler, B. (2009) Major surface protein LipL32 is not required for either acute or chronic infection with *Leptospira interrogans*.. *Infect. Immun. 77*, 952–958.
47. Espenel, C., Giocondi, M. C., Seantier, B., Dosset, P., Milhiet, P. E., and Le Grimellec, C. (2008) Temperature-dependent imaging of living cells by AFM. *Ultramicroscopy 108*, 1174–1180.
48. Müller, D. J., Helenius, J., Alsteens, D., and Dufrêne, Y. F. (2009) Force probing surfaces of living cells to molecular resolution. *Nat. Chem. Biol. 5*, 383–390.
49. Takeda, K., and Akira, S. (2004) TLR signaling pathways. *Semin. Immunol. 16*, 3–9.
50. Gerold, G., Ajaj, K. A., Bienert, M., Laws, H. J., Zychlinsky, A., and de Diego, J. L. (2008) A Toll-like receptor 2-integrin β3 complex senses bacterial lipopeptides via vitronectin. *Nat. Immunol. 9*, 761–768.